Journal of Solid State Chemistry **154,** 246–253 (2000)
doi:10.1006/jssc.2000.8844, available online at http://www.idealibrary.com on IDEAL®

Polyborides with Th_2NiB_{10}-Type Structure: Synthesis, Crystal Structure, and Magnetic and Electrical Properties

Wolfgang Jeitschko, Thomas Konrad, Klaus Hartjes, Arne Lang, and Rolf-Dieter Hoffmann

Anorganisch-Chemisches Institut, Universität Münster, Wilhelm-Klemm-Strasse 8, D-48149 Münster, Germany

Received September 9, 1999; accepted December 21, 1999

The new rare-earth nickel polyborides R_2NiB_{10} (R = Y, Ce–Nd, Sm, Gd–Ho) were prepared by reacting cold-pressed pellets of the elemental components in an arc-melting furnace, followed by annealing in evacuated silica tubes. They crystallize with the orthorhombic Th_2NiB_{10}-type structure, which was refined from X-ray powder diffractometer data of Ce_2NiB_{10} (a = 565.4(1) pm, b = 1125.8(2) pm, c = 419.6(1) pm) and Nd_2NiB_{10} (a = 561.4(1) pm, b = 1119.2(2) pm, c = 417.7(1) pm). The magnetic properties of these polyborides and also of Th_2CoB_{10} and Th_2NiB_{10} were determined with a superconducting quantum interference magnetometer between 2 and 400 K with magnetic flux densities up to 5.5 T. Y_2NiB_{10}, Th_2CoB_{10}, and Th_2NiB_{10} are Pauli paramagnetic. The others show Curie–Weiss behavior with magnetic moments corresponding to those of the free R^{3+} ions, with the exception of Ce_2NiB_{10}, where cerium has a mixed valence and Sm_2NiB_{10} with the van Vleck paramagnetic Sm^{3+} ion. Antiferromagnetic order was observed for the compounds R_2NiB_{10} (R = Pr, Nd, Sm, Gd–Ho) with Néel temperatures ranging between 8 K for Pr_2NiB_{10} and 33 K for Gd_2NiB_{10}. Tb_2NiB_{10}, Dy_2NiB_{10}, and Ho_2NiB_{10} are metamagnetic. Electrical resistivity measurements reflect the magnetic ordering temperatures and indicate metallic behavior for all compounds.

INTRODUCTION

Three new thorium transition metal polyborides Th_2TB_{10} (T = Fe, Co, Ni) were reported recently (1). They crystallize with a new structure type, which was determined for Th_2NiB_{10}. The structure is closely related to that of CaB_6, which had also been found for the rare earth borides RB_6 and ThB_6 (2). In the ternary compounds Th_2TB_{10} two of the linking boron atoms of adjacent B_6 octahedra are replaced for one-sixth of the boron atoms by a transition metal atom. In the present communication we report the isotypic rare-earth nickel polyborides R_2NiB_{10} and their physical properties. A preliminary account on the preparation and the crystal structure of these compounds has been given at a conference (3).

EXPERIMENTAL

Sample Preparation

The samples were prepared by arc-melting of cold-pressed pellets and subsequent annealing. Starting materials were ingots of the rare-earth metals (nominal purities all equal or greater than 99.9%) and powders of nickel (99.9%) and boron (99%). Filings of the rare-earth elements were prepared under dried (sodium) paraffin oil. Adhering iron particles were removed with a magnet. The oil was washed out by treatment with dry hexane. The filings (especially those of the light rare-earth elements) were not allowed to contact air prior to the sample preparation. The pellets, with a total weight of about 250 mg, were arc-melted from both sides in purified argon to enhance the homogeneity of the buttons, which subsequently were wrapped in tantalum foil, annealed in evacuated silica tubes for 10 days at 1100°C, and quenched in water.

The annealed buttons were easily ground to fine powders, which are not sensitive to the air. Energy-dispersive X-ray fluorescence analyses in a scanning electron microscope did not reveal any impurity elements heavier than sodium.

Powder Diffractometry

Guinier powder diagrams were recorded with Cu$K\alpha_1$ radiation using α-quartz (a = 491.30 pm, c = 540.46 pm) as an internal standard. Indices were assigned on the basis of the calculated (4) powder patterns using the positional parameters of the Th_2NiB_{10}-type structure (1). The lattice constants (Table 1) were refined by least-squares fits.

The crystal structures of Ce_2NiB_{10} and Nd_2NiB_{10} were refined from X-ray powder data using a STADI P diffractometer, Ge(111) monochromated Cu$K\alpha_1$ radiation, and flat rotating samples in the symmetric transmission mode with a linear position-sensitive detector. Intensity data points (n = 4500) were recorded for each sample in the 2θ range between 5° and 95° with a step width of 0.02°.

The structures were refined with the Rietveld least-squares program FULLPROF (5) using the atomic scattering

0022-4596/00 $35.00

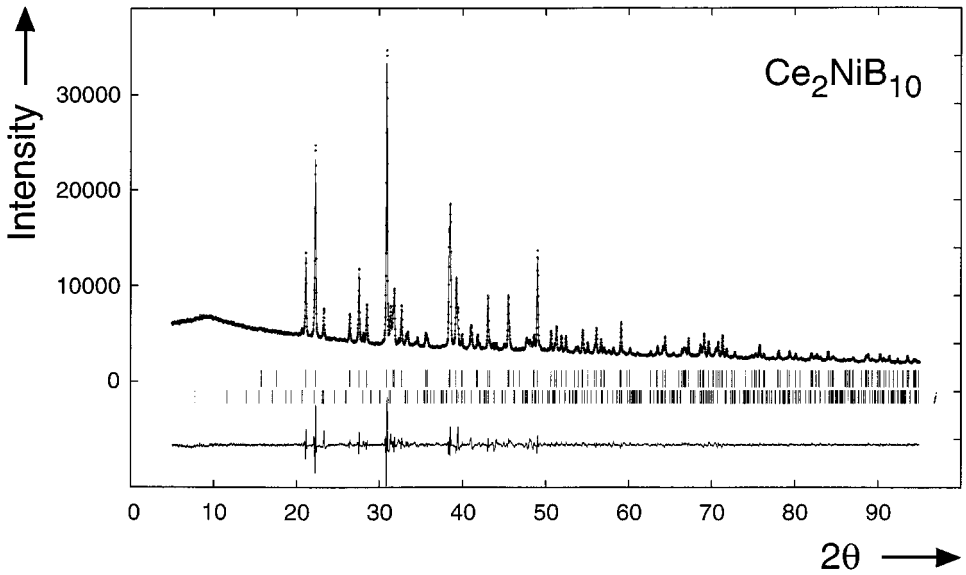

FIG. 1. Powder diffraction diagram of Ce_2NiB_{10} as recorded with Cu$K\alpha_1$ radiation. In the top part of the figure the observed (dots) and calculated pattern (continuous line) is presented. The calculated line positions are indicated by vertical bars and the difference pattern is shown below. The calculated line positions for an orthorhombic impurity phase (i) are also indicated.

factors provided by the program. The starting positional parameters were taken from the single-crystal structure determination of Th_2NiB_{10} (1). The profiles were fitted with a pseudo-Voigt function and four variable profile parameters. In both experimental patterns small amounts of different impurity phases were detected. Both of these could be indexed with orthorhombic cells, which were refined together with the structures of the borides Ce_2NiB_{19} and Nd_2NiB_{10}, respectively. As an example the evaluation of the diagram of the Ce_2NiB_{10} sample is shown in Fig. 1. The following lattice constants were obtained for Ce_2NiB_{10} and Nd_2NiB_{10}: $a = 565.39(1)$ pm, $b = 1125.69(1)$ pm, $c = 420.13(1)$ pm and $a = 562.51(2)$ pm, $b = 1120.70(4)$ pm, $c = 418.20(1)$ pm, respectively. These lattice constants are in good agreement with those determined from the Guinier data (Table 1). However, we believe the latter to be more reliable, because they were determined relative to an internal standard as already discussed.

SQUID Magnetometry

The magnetic properties of the new compounds were investigated with a SQUID (superconducting quantum interference device) magnetometer. The samples of R_2NiB_{10} with R = Y, Ce, Pr, Nd, and Sm contained very small amounts of ferromagnetic impurities, as was indicated by the field-dependence of their magnetic susceptibilities

TABLE 1
Lattice Constants of Borides Crystallizing with the Orthorhombic Th_2NiB_{10}-Type Structure[a]

Compound	a (pm)	b (pm)	c (pm)	V (nm^3)
Y_2NiB_{10}	555.7(1)	1110.9(2)	415.0(1)	0.2562
Ce_2NiB_{10}	565.4(1)	1125.8(1)	419.6(5)	0.2671
Pr_2NiB_{10}	561.9(2)	1122.7(3)	419.2(1)	0.2645
Nd_2NiB_{10}	561.4(1)	1119.2(2)	417.7(1)	0.2624
Sm_2NiB_{10}	560.5(2)	1113.3(2)	417.7(1)	0.2606
Gd_2NiB_{10}	557.6(1)	1111.9(3)	414.9(1)	0.2572
Tb_2NiB_{10}	555.6(2)	1110.9(5)	415.0(1)	0.2561
Dy_2NiB_{10}	554.9(2)	1109.4(2)	414.4(1)	0.2551
Ho_2NiB_{10}	554.5(4)	1108.6(4)	413.9(2)	0.2544

[a] Standard deviations in the place values of the least significant digits are listed in parentheses throughout the paper.

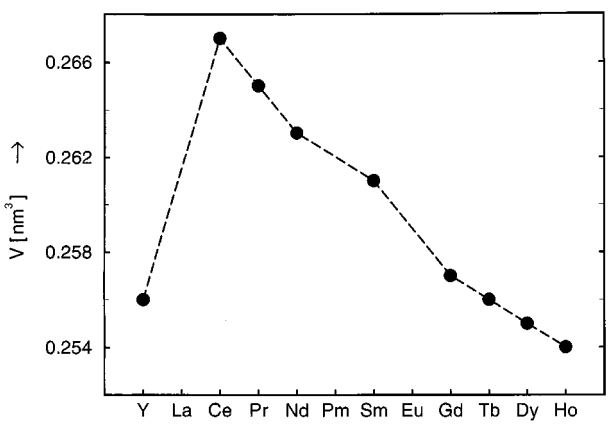

FIG. 2. Cell volumes of the rare-earth nickel polyborides R_2NiB_{10}.

TABLE 2
Magnetic Properties of Th_2NiB_{10}-Type Borides[a]

Compound	Magnetic property	Θ (K)	T_N (K)	μ_{exp} (μ_B)	$\mu_{eff}(R^{3+})$ (μ_B)	T_E (K)
Y_2NiB_{10}	Pauli paramagnetic	—	—	—	—	—
Ce_2NiB_{10}	Mixed valent?	− 34(2)	—	2.03(3)	2.54	20(4)
Pr_2NiB_{10}	Antiferromagnetic	− 27(2)	8(4)	3.51(2)	3.58	19(3)
Nd_2NiB_{10}	Antiferromagnetic	− 20(3)	9(1)	3.03(3)	3.62	10(2)
Sm_2NiB_{10}	Van Vleck paramagnetic and antiferromagnetic	—	11(1)	1.82(2)	1.78	12(2)
Gd_2NiB_{10}	Antiferromagnetic	− 28(3)	33(2)	7.31(5)	7.94	31(2)
Tb_2NiB_{10}	Metamagnetic	− 27(3)	25(2)	8.92(9)	9.72	25(2)
Dy_2NiB_{10}	Metamagnetic	− 13(1)	21(2)	9.77(7)	10.63	13(3)
Ho_2NiB_{10}	Metamagnetic	− 7(1)	11(1)	9.16(2)	10.60	12(2)
Th_2CoB_{10}	Pauli paramagnetic	—	—	—	—	—
Th_2NiB_{10}	Pauli paramagnetic	—	—	—	—	—

[a] Listed are the paramagnetic Curie temperatures (Weiss constants) Θ and the Néel temperatures T_N. The experimentally determined effective magnetic moments per rare-earth atom μ_{exp} were obtained by evaluation of the $1/\chi$ vs T plots at high temperatures according to $\mu_{exp} = 2.83[(\chi_{cgs}/2)\cdot(T-\Theta)]^{1/2}\mu_B$. They are compared with the corresponding theoretical moments μ_{eff} calculated from the relation $\mu_{eff} = g\cdot[J\cdot(J+1)]^{1/2}\,\mu_B$, where g is the Landé factor and J the total angular momentum number (8). In the last column the temperatures of the discontinuities T_E in the electrical conductivity plots are listed (see text).

already at room temperature. The amounts of these impurities, however, were so small that the susceptibility values recorded with magnetic flux densities of 3 and 5 T were practically identical in all cases, and no extrapolations to infinite magnetic field strengths were needed.

The powdered samples with weights of approximately 30 mg were placed in silica tubes (i.d. 2 mm, o.d. 3 mm) and compressed with cellulose in order to prevent the movements of small particles in the applied magnetic fields. Usually the samples were cooled to liquid helium temperature without an applied magnetic field. The temperature dependencies of the susceptibility data were then recorded in the desired magnetic fields while the samples were heated or cooled, respectively.

Electrical Resistivity Measurements

The temperature dependence of the electrical conductivity of all new compounds was determined with the four-probe method as described by van der Pauw (6). Compact fragments of the polycrystalline arc-melted and annealed buttons of about 0.5 mm diameter were contacted by four copper filaments (30 μm diameter) using a single-component polyimide glue with suspended silver particles. The solidification of this glue was achieved by heating the samples to 150°C for 10 s. After this treatment the contacted samples were sealed in a transparent two-component cement to prevent their accidental mechanic destruction. The samples were then placed into a dewar with liquid helium together with an attached thermocouple. The temperature was varied by slowly moving the sample holder into or out of the helium dewar.

RESULTS AND DISCUSSION

The cell volumes of the new borides with Th_2NiB_{10} type structure are plotted in Fig. 2. They show the expected lanthanoid contraction. We were not successful in preparing the corresponding lanthanum and erbium compounds. The cerium compound has a cell volume which fits the extrapolation of the volumes for the other compounds, where the rare-earth atoms are trivalent. Hence, the cerium atoms in Ce_2NiB_{10} are expected to be (at least predominantly) trivalent. This is further discussed below. The yttrium compound has a cell volume which is practically the same as that of the terbium compound. This matches the trend

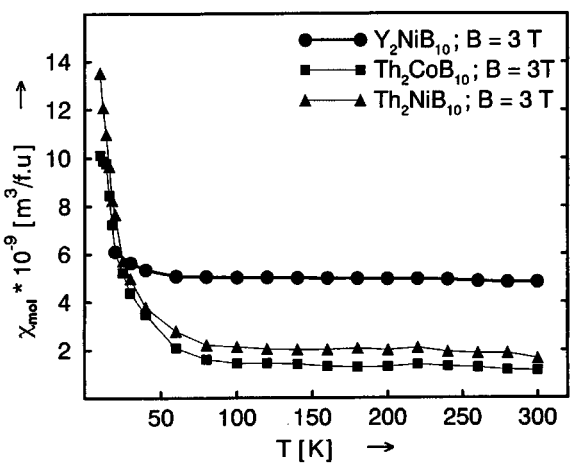

FIG. 3. Magnetic susceptibility of the Paul paramagnets Y_2NiB_{10}, Th_2CoB_{10}, and Th_2NiB_{10}. The upturns of the susceptibilities at low temperatures are ascribed to paramagnetic impurities or surface states.

observed for rare-earth carbides, where the volumes of the yttrium compounds fit between those of the terbium and holmium compounds, while in oxides the cell volumes of the yttrium compounds generally are in between those of the corresponding dysprosium and erbium compounds (7).

The magnetic properties of the ternary borides are summarized in Table 2. The magnetic susceptibilities of the compounds with the nonmagnetic R components yttrium and thorium show very low magnetic susceptibilities, which are nearly temperature-independent (Fig. 3), as is typical for Pauli paramagnetism. The increase of the magnetic

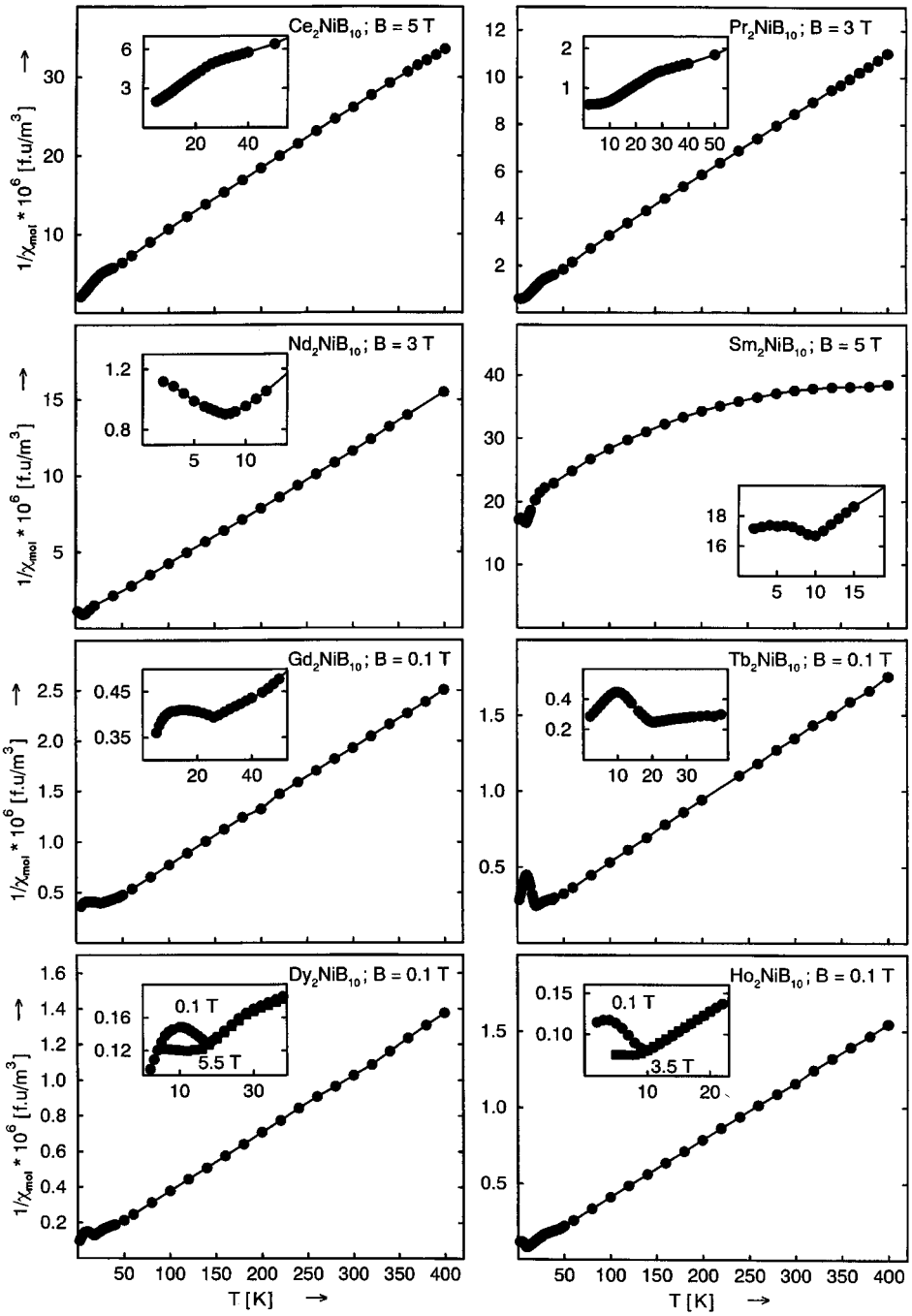

FIG. 4. Reciprocal susceptibilities of the rare-earth nickel polyborides R_2NiB_{10} as measured with the indicated magnetic flux densities. (Insets) Behavior at low temperatures. Because of a calibration error the plots at low temperatures (between 8 and 50 K) are shifted to slightly lower temperatures; the Néel temperatures given in Table 2 are correct.

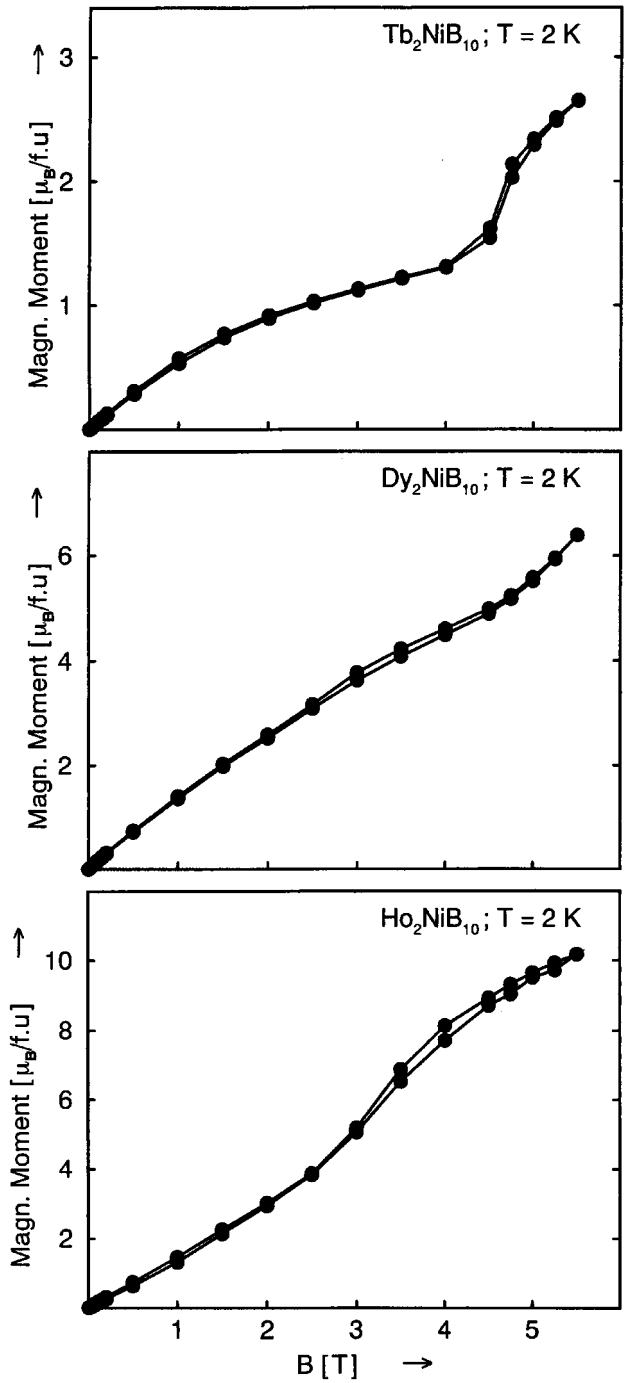

FIG. 5. The magnetization behavior of the three metamagnets Tb_2NiB_{10}, Dy_2NiB_{10}, and Ho_2NiB_{10} recorded at a temperature of 2 K.

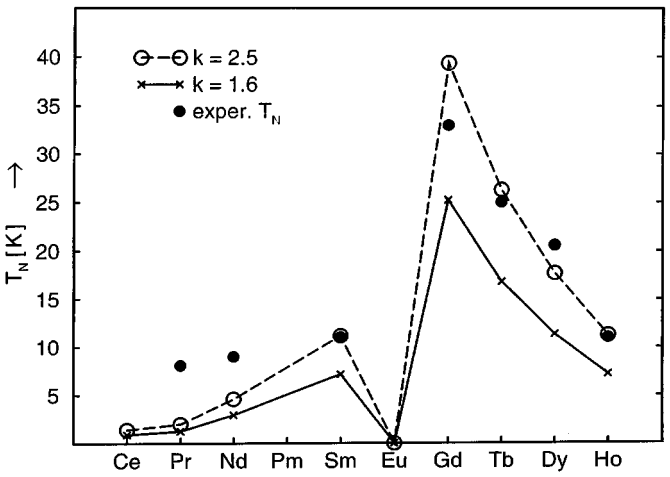

FIG. 6. Comparison of the experimentally determined magnetic ordering temperatures with those calculated for two de Gennes functions with the k values 1.6 and 2.5.

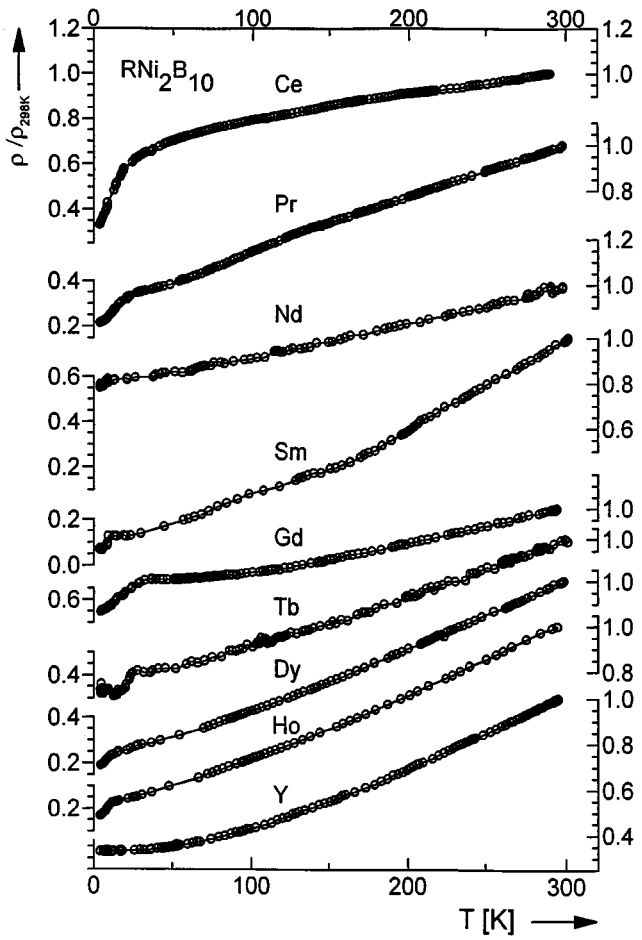

FIG. 7. Temperature dependence of the electrical resistivities of several rare-earth nickel polyborides R_2NiB_{10}. The room temperature resistivities varied between the values of 30 and 300 $\mu\Omega \cdot$ cm. Because of the large error limits of these values only the relative resistivities are shown.

susceptibilities for the compounds Y_2NiB_{10}, Th_2CoB_{10}, and Th_2NiB_{10} below 100 K may be ascribed to magnetic impurities or magnetic surface states. Such "Curie tails" are frequently observed for Pauli paramagnets. Much higher susceptibility values (about 10 to 100 times greater) would

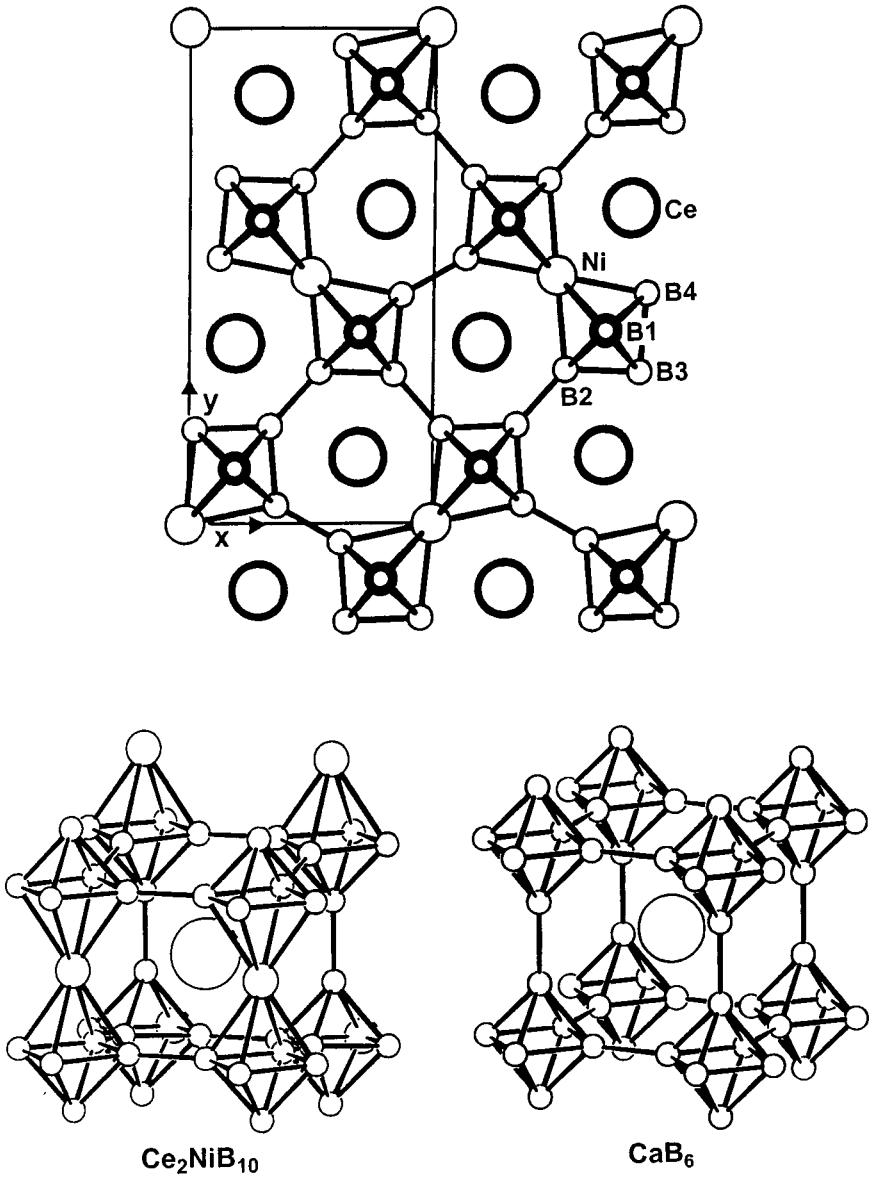

FIG. 8. Crystal structure of Ce_2NiB_{10}. (Top) Projection of the structure along the short c axis. (Bottom) A cutout of the structure is compared to the cubic structure of CaB_6. The large cerium atoms fill the voids of a three-dimensional network of the nickel and boron atoms. Note that the nickel atoms replace two boron atoms of adjacent boron octahedra.

be expected for compounds with magnetic moments carried by the cobalt or nickel atoms.

The magnetic properties of the borides R_2NiB_{10} with the magnetic rare earth elements are dominated by the magnetism of these elements. The reciprocal susceptibilities of Ce_2NiB_{10} (Fig. 4) obey the Curie–Weiss law. The magnetic moment of $\mu_{exp} = 2.03(3)\ \mu_B$ obtained from the straight portion of the $1/\chi$ vs T plot above 100 K is somewhat lower than the theoretical moment of $\mu_{eff} = 2.54\ \mu_B$ calculated for Ce^{3+}. This suggests that the cerium atoms in this compound might have a mixed Ce^{3+}/Ce^{4+} valency (the theoretical moment for Ce^{4+} is zero). However, as can be seen from Table 2, for most compounds the experimental moments are slightly lower than the theoretical ones. Also, the plot of the cell volumes (Fig. 2) does not show a deviation from the curve to a smaller value for the cerium compound, as would be expected, if the cerium atoms were tetravalent. Nevertheless, we cannot exclude the possibility that a small portion of the cerium atoms is tetravalent.

The reciprocal susceptibilities of the compounds R_2NiB_{10} with R = Pr, Nd, Gd, Tb, Dy, and Ho show a linear temperature dependence above 100 K (Fig. 4) with Weiss constants

TABLE 3
Atomic Parameters of Ce_2NiB_{10} and Nd_2NiB_{10}[a]

Atom	*Pbam*	*x*	*y*	*z*	B[a]
Ce_2NiB_{10}					
Ce	4*h*	0.1911(3)	0.3633(2)	$\frac{1}{2}$	1.93(5)
Ni	2*a*	0	0	0	1.7(2)
B1	8*i*	0.212(4)	0.115(2)	0.313(3)	0.6
B2	4*g*	0.056(5)	0.184(3)	0	0.6
B3	4*g*	0.350(6)	0.190(2)	0	0.6
B4	4*g*	0.380(5)	0.036(3)	0	0.6
Nd_2NiB_{10}					
Nd	4*h*	0.1937(3)	0.3628(2)	$\frac{1}{2}$	0.95(4)
Ni	2*a*	0	0	0	2.2(2)
B1	8*i*	0.214(4)	0.127(3)	0.345(3)	0.6
B2	4*g*	0.065(6)	0.181(3)	0	0.6
B3	4*g*	0.321(7)	0.182(2)	0	0.6
B4	4*g*	0.364(7)	0.038(3)	0	0.6

[a] The isotopic displacement parameters B ($\times 10^4$ pm^2) of the boron positions were not refined.

Θ varying between $-7(1)$ K for Ho_2NiB_{10} and $-28(3)$ K for Gd_2NiB_{10}, suggesting antiferromagnetic order at low temperatures. The Néel temperatures T_N were estimated from the minima in the reciprocal susceptibility curves. They vary between 8(4) K for Pr_2NiB_{10} and 33(2) K for Gd_2NiB_{10}. The antiferromagnetism of these compounds was confirmed by magnetization measurements. No metamagnetic transitions were observed for Pr_2NiB_{10}, Nd_2NiB_{10}, and Gd_2NiB_{10} up to magnetic flux densities of 5.5 T, the highest flux densities obtainable with our magnetometer. In contrast, metamagnetism was found for the three borides, Tb_2NiB_{10}, Dy_2NiB_{10}, and Ho_2NiB_{10} (Fig. 5), with critical field strengths of about 4 T for Tb_2NiB_{10} and 3 T for Dy_2NiB_{10} and Ho_2NiB_{10}. The highest magnetizations reached at 5.5 T were 2.65(1) μ_B/formula unit (f.u.), 6.40(2) μ_B/f.u., and 10.18(4) μ_B/f.u. for Tb_2NiB_{10}, Dy_2NiB_{10}, and Ho_2NiB_{10}, respectively. These values are considerably lower than the theoretical saturation moments (calculated according to $\mu_{calc(sm)} = g \cdot J$) of 2×9.0, 2×10.0, and 2×10.0 μ_B/f.u., respectively, thus indicating that the saturation moments are not yet reached at the highest obtainable magnetic flux density of 5.5 T. Also the samples contained small amounts of impurities, which were not considered during the evaluations of the experimental data.

Antiferromagnetic order was also indicated for Sm_2NiB_{10} with a Néel temperature of 11(1) K (Fig. 4). Above this temperature, however, the reciprocal susceptibility of this compound does not obey the Curie–Weiss law, as is frequently observed for samarium compounds. The Sm^{3+} ion is known to show van Vleck paramagnetism. The magnetic moment μ_{exp} calculated from the magnetic susceptibility χ according to the relation $\mu_{exp} = 2.83\ [(\chi_{cgs}/2) \times T]^{1/2}$ μ_B for $T = 400$ K amounted to 1.82(2) μ_B. This value compares well with the theoretical value $\mu_{eff} = 1.78$ μ_B calculated from van Vleck's formula (9) with a screening constant of $\sigma = 33$.

In Fig. 6 we have plotted the Néel temperatures of the compounds R_2NiB_{10} (R = Ce–Nd, Sm, Gd–Ho) as compared to the de Gennes function (10), calculated for two k values. It can be seen that the experimental Néel temperatures do not fit very well this theoretical function. This indicates that the antiferromagnetic structures of these borides are not the same.

The electrical resistivities of all borides with the exception of those of the thorium compounds were investigated as a function of temperature. The resistivities of these compounds increase with temperature, as is typical for

TABLE 4
Interatomic Distances in the Structures of the Borides Ln_2NiB_{10} (Ln = Ce, Nd)[a]

	Ce/Nd		Ce/Nd		Ce/Nd		Ce/Nd
Ln: 2B1	284/277	Ni: 2B2	210/206	B2: 1B3	166/144	B4: 1B4	158/174
2B4	289/288	2B4	219/209	2B1	176/177	1B3	174/163
2B1	291/272	4B1	220/236	1B3	184/206	2B1	185/195
2B3	292/300	4*Ln*	314/311	1Ni	210/206	1Ni	219/209
2B4	296/301	B1: 1B1	157/130	2*Ln*	299/299	2*Ln*	289/288
2B1	299/308	1B3	175/168	2*Ln*	301/301	2*Ln*	296/301
2B2	299/299	1B2	176/177	B3: 1B2	166/144		
2B3	300/300	1B4	185/195	1B4	174/163		
2B2	301/301	1Ni	220/236	2B1	175/168		
2B1	306/299	1*Ln*	284/272	1B2	184/206		
2Ni	314/311	1*Ln*	291/277	2*Ln*	292/300		
1*Ln*	376/376	1*Ln*	299/299	2*Ln*	300/300		
2*Ln*	381/378	1*Ln*	306/308				
2*Ln*	420/418						

[a] All distances shorter than 420 pm (metal–metal, *Ln*–B), 300 pm (Ni–B), and 240 pm (B–B) are listed. The standard deviations are all equal or less than 6 pm.

metallic conductors (Fig. 7). Between liquid helium and room temperature the resistivities increase by factors of about 2 to 10. The lowest increases were observed for Nd_2NiB_{10} and Gd_2NiB_{10}, and the highest for Sm_2NiB_{10}. The absolute values are about 100 to 200 $\mu\Omega \cdot$ cm at room temperature. These values are higher than those of typical metals, e.g., elemental iron or nickel, by a factor of about 20 (11).

At low temperatures the electrical resistivities show some structure for all investigated borides R_2NiB_{10} with the exception of Y_2NiB_{10}, where the yttrium atoms do not carry magnetic moments. In coming from high temperatures the first discontinuities in the electrical resistivity curves T_E correlate roughly with the Néel temperatures T_N. As can be seen from Table 2 the agreement between the visually estimated T_N and T_E values is good in general with the exceptions for the praseodymium and dysprosium compounds.

The results of our structure refinements of Ce_2NiB_{10} are summarized in Tables 3 and 4. The crystal structure of these Th_2NiB_{10}-type borides is shown in Fig. 8 with Ce_2NiB_{10} as representative. As can be seen, it has great similarity with that of CaB_6. The latter structure has been found for the binary rare-earth borides RB_6 and for ThB_6 (2). Our structure refinements for Ce_2NiB_{10} and Nd_2NiB_{10} from X-ray powder data unambiguously prove the isotypy of the structures of these ternary rare-earth nickel borides with that of Th_2NiB_{10}. The latter structure has been determined from single-crystal X-ray data not only for the nickel compound but also for the isotypic compounds Th_2FeB_{10} and Th_2CoB_{10} (1). As could be expected, our present refinements from powder data are not as accurate. However, the major trends are reproduced. For instance, the B–B bonds between neighboring NiB_5 octahedra are shorter than the B–B bonds within an octahedron. The average B–B bonds within the NiB_5 octahedra are 179 and 180 pm for Ce_2NiB_{10} and Nd_2NiB_{10}, respectively, as compared to the corresponding average value of 177.1 pm in the thorium compounds Th_2TB_{10} (T = Fe, Co, Ni). The B–B bonds bridging two octahedra are considerably shorter; in Ce_2NiB_{10} and Nd_2NiB_{10} they are 149 pm on average, as compared to the average of 167 pm in the three thorium compounds. The same tendency is observed in the structures of the binary borides LaB_6 (12), ThB_6 (13), and ThB_4 (13), which all have been refined from single-crystal X-ray data. In these compounds the B–B bonds between B_6 octahedra are 166, 161, and 167 pm, respectively, while the B–B bonds within the B_6 octahedra are 177 pm, 176 pm, and, on average, 181 pm for LaB_6, ThB_6, and ThB_4, respectively.

ACKNOWLEDGMENTS

We thank Mr. K. Wagner for the work at the scanning electron microscope and Dr. G. Höfer (Heraeus Quarzschmelze) for a generous gift of silica tubes. This work was also supported by the Deutsche Forschungsgemeinschaft, the Fonds der Chemischen Industrie, and the International Centre for Diffraction Data.

REFERENCES

1. T. Konrad and W. Jeitschko, *Z. Naturforsch.* **50b,** 1195 (1995).
2. P. Villars and L. D. Calvert, "Pearson's Handbook of Crystallographic Data for Intermetallic Compounds," 2nd ed. ASM International, Materials Park, OH, 1991.
3. T. Konrad and W. Jeitschko, *Z. Kristallogr. Suppl.* **9,** 192 (1995).
4. K. Yvon, W. Jeitschko, and E. Parthé, *J. Appl. Crystallogr.* **10,** 73 (1977).
5. J. Rodriguez-Carvajal, "FULLPROF: A Program for Rieveld Refinement and Profile Matching Analysis of Complex Powder Diffraction Patterns." Grenoble, Institut Laue-Langevin, 1991.
6. L. J. van der Pauw, *Phillips Res. Rep.* **13,** 1 (1958).
7. W. Jeitschko, G. Block, G. E. Kahnert, and R. K. Behrens, *J. Solid State Chem.* **89,** 191 (1990).
8. S. Legvold, *in* "Ferromagnetic Materials," (E. P. Wohlfarth, Ed.), Vol. 1, pp. 183–295. North Holland, Amsterdam, 1980.
9. J. H. van Vleck, "The Theory of Electric and Magnetic Susceptibilities." Oxford Univ. Press, London, 1932.
10. P.-G. de Gennes, *C. R. Acad. Sci. Paris* **247,** 1836 (1958).
11. R. C. Weast (Ed.), "Handbook of Chemistry and Physics," 59th ed. CRC Press, Boca Raton, FL, 1978.
12. M. M. Korsukova, V. N. Gurin, T. Lundström, and L.-E. Tergenius, *J. Less-Common Metals* **117,** 73 (1986).
13. T. Konrad, W. Jeitschko, M. E. Danebrock, and C. B. H. Evers, *J. Alloys Compd.* **234,** 56 (1996).